THE JOURNAL OF PHYSICAL CHEMISTRY A

Article

pubs.acs.org/JPCA

Investigation of Terahertz Vibration−Rotation Tunneling Spectra for the Water Octamer

Jeremy O. Richardson,[†,§] David J. Wales,[†] Stuart C. Althorpe,*[,†] Ryan P. McLaughlin,[‡,∥] Mark R. Viant,[‡,⊥] Orion Shih,[‡] and Richard J. Saykally*[,‡]

[†]Department of Chemistry, University of Cambridge, Lensfield Road, Cambridge, CB2 1EW, United Kingdom

[‡]Department of Chemistry, University of California, Berkeley, California 94720, United States

Supporting Information

ABSTRACT: We report a combined theoretical and experimental study of the water octamer-h16. The calculations used the ring-polymer instanton method to compute tunnelling paths and splittings in full dimensionality. The experiments measured extensive high resolution spectra near 1.4 THz, for which isotope dilution experiments and group theoretical analysis support assignment to the octamer. Transitions appear as singlets, consistent with the instanton paths, which involve the breakage of two hydrogen-bonds and thus give tunneling splittings below experimental resolution.

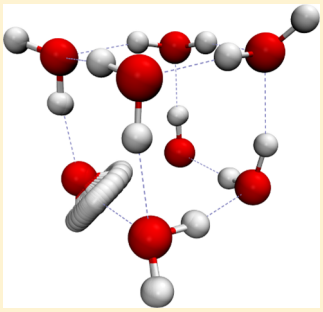

INTRODUCTION

The advent of far-infrared or terahertz vibration−rotation tunneling (VRT) spectroscopy[1−5] stimulated numerous experimental and theoretical studies of water clusters addressing the dimer, trimer, tetramer, pentamer, and hexamer, which we will not attempt to review here. The water octamer has been the subject of a number of theoretical investigations since early simulations by Tsai and Jordan,[6,7] Stillinger and David,[8] and Brink and Glasser.[9] The "melting" transition in this finite system was analyzed by Wales and Ohmine in terms of the underlying potential energy landscape,[10] and rearrangement mechanisms were characterized between a number of low-lying isomers.[11] More recent work has shown that the solid-like and liquid-like forms of this cluster can be distinguished using an order parameter based on bond orientation.[12,13] Both empirical potentials[6,7,11,14−16] and studies that include explicit treatment of the electronic structure[17,18] identify two particularly low-energy cuboidal structures with S_4 and D_{2d} symmetries, which dominate the solid-like phase. For example, with the TIP4P potential,[19] these two isomers are the only ones possessing any significant occupation probability below about 160 K.[10,12,13,20] In the liquid-like phase, a large number of noncuboidal structures are sampled, along with higher energy cuboids.[7,10,13,21−23]

The S_4 and D_{2d} isomers have been partially characterized by mid-IR vibrational spectroscopy,[24−26] and the stability of these octameric structures is further reflected by their presence in a diverse range of crystal structures.[27−31] Various theoretical studies have investigated properties ranging from photoabsorption,[32] electron attachment,[33] and the behavior in nonpolar cavities.[34] The evolution of the thermodynamic properties[20] and the underlying potential energy landscape[35] have also been investigated as a function of a static applied electric field. At high field strengths, extended structures become favorable, and the average number of hydrogen-bonds decreases. Various size-dependent properties[36] have been considered, such as the ionic product of water[37] and charge separation.[38]

In the present work, we employ a new ring-polymer instanton method[39,40] to estimate the magnitude of tunneling splittings in the S_4 and D_{2d} isomers of the water octamer. The pathways that correspond to the largest splittings are identified, and these values are found to lie below the resolution of current experiments. Both the S_4 and D_{2d} isomers are therefore expected to behave as semirigid symmetric top molecules. This new information is used here to tentatively assign a partial band observed near 1.4 THz to VRT transitions in the water octamer.

THE RING-POLYMER INSTANTON METHOD

Here we summarize the ring-polymer instanton method,[39,40] which was used to compute approximate tunneling splittings and tunneling pathways. The basis of the approach is that the tunneling splittings can be obtained from the limit[41−43]

$$\lim_{\beta\to\infty}\frac{Q(\beta)}{Q_0(\beta)}=\frac{1}{G}\sum_{\nu=1}^{G}e^{-\beta(E_\nu-E_0)} \quad (1)$$

where $Q(\beta)$ and $Q_0(\beta)$ are the partition functions of the system with and without inclusion of tunneling, $\beta = 1/k_BT$, E_0 is the

Special Issue: Joel M. Bowman Festschrift

Received: November 15, 2012

   dx.doi.org/10.1021/jp311306a | J. Phys. Chem. A XXXX, XXX, XXX−XXX

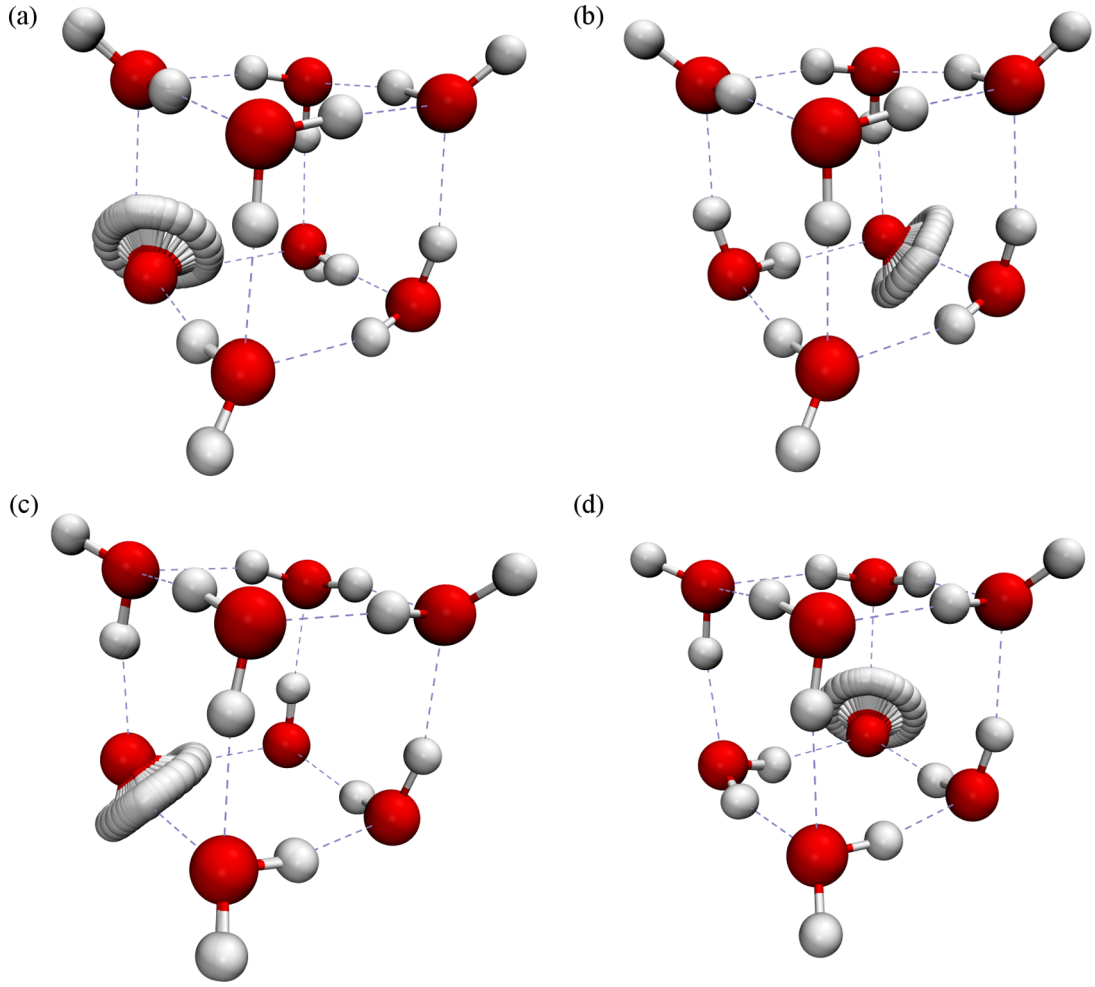

Figure 1. Conflated snapshots of instanton tunneling paths (kinks) for the water octamer. The paths show the (a) D_{2d}(ADD), (b) D_{2d}(DAA), (c) S_4(ADD), and (d) S_4(DAA) rearrangements, and were computed as described in the text.

ground state energy of the system in the absence of tunneling, and E_ν are the energy levels that result from tunneling between the G degenerate potential wells of the system, corresponding to nonsuperimposable permutation-inversion isomers.

The ring-polymer instanton method approximates the ratio in eq 1 by representing $Q(\beta)$ and $Q_0(\beta)$ using ring-polymer phase-space integrals, and then evaluates the integrals by steepest descent about the dominant "instanton" tunneling paths.[44−47] These paths become infinitely long in the limit $\beta \to \infty$, and there are an infinite number of them, describing all the possible ways in which the system can follow paths between different sequences of minima. However, a straightforward application of graph theory allows one to obtain the tunneling-splitting pattern from the *tunneling matrix*, **W**, defined by

$$\mathbf{W}_{\lambda\mu} = \mathbf{A}_{\lambda\mu} h_{\lambda\mu} \tag{2}$$

in which the adjacency matrix **A** describes the number of paths connecting well λ to well μ (where $\lambda,\mu = 1,...,G$), and

$$h_{\lambda\mu} = -\frac{\hbar}{\Phi}\sqrt{\frac{S_{\lambda\mu}}{2\pi\hbar}}\, e^{-S_{\lambda\mu}/\hbar} \tag{3}$$

The action, $S_{\lambda\mu}$, is obtained by minimizing $\beta_N \hbar U_N(\beta,\mathbf{x})$, in the limits $\beta \to \infty$ and $\beta_N \to 0$, where $\beta_N = \beta/N$ and the potential energy,

$$U_N(\beta, \mathbf{x}) = \sum_{i=1}^{N} V(x_{i,1}, ..., x_{i,f}) + \sum_{j=1}^{f} \frac{m_j}{2(\beta_N\hbar)^2} \times [(x_j^\lambda - x_{N,j})^2 + \sum_{i=1}^{N-1} (x_{i+1,j} - x_{i,j})^2 + (x_{1,j} - x_j^\mu)^2] \tag{4}$$

is that of a (fictitious) linear polymer, consisting of a sequence of N replicas of the f-dimensional system, each described by a set of coordinates $\{x_{i,1},...,x_{i,f}\}$ and potential energy surface $V(x_1,...,x_f)$. The replicas are joined by Hooke's-law springs and extend along the tunneling path. In practice, β and N are treated as convergence parameters, and the linear polymer is gradually cooled down until the resulting action $S_{\lambda\mu}$ has converged. $S_{\lambda\mu}$ then corresponds to the dominant "instanton" tunneling path connecting wells λ and μ. The factor Φ in eq 3 is obtained as explained in ref 39, and describes the effect of fluctuations around each dominant path. The paths and the resulting matrix elements $h_{\lambda\mu}$ are computed for all "feasible" tunneling paths connecting the various minima.[48] A path is deemed to be unfeasible if the action $S_{\lambda\mu}$ is too large to produce an observable tunneling splitting pattern. This regime can be deduced either by inspection of the potential surface (e.g., if the only available path involves the breaking of several hydrogen-bonds), or by running an approximate calculation with only a

dx.doi.org/10.1021/jp311306a | J. Phys. Chem. A XXXX, XXX, XXX−XXX

relatively small number of beads and a low value of β. The energy levels, E_ν, and hence the tunneling splitting pattern, are then obtained by diagonalizing **W**.

The main approximation made in the instanton approach is that fluctuations around the instanton tunneling paths can be treated harmonically (i.e., the "steepest-descent" approximation). However, the crucial anharmonicity along the tunneling path is included in full. An additional approximation is that the rotational motion is approximately separable from the tunneling motion. Hence the approach will break down when there is strong dependence of rotational quantum numbers on the tunneling motion (e.g., in acceptor tunneling in water dimer).[40] The instanton method is therefore expected to give order-of-magnitude estimates of the tunneling splittings and to be useful for predicting the dominant tunneling paths and the structure of the splitting pattern. However, in tests on water dimer and trimer,[40] the instanton approach performed significantly better than this, giving results that were in almost quantitative agreement with experiment for $(D_2O)_2$ using the HBB2 potential of Bowman and co-workers.[49]

THEORETICAL PREDICTIONS FOR THE WATER OCTAMER

The water octamer has two low-lying wells, which have the cuboidal D_{2d} and S_4 geometries shown in Figure 1. The presence of the S_4 symmetry element in both isomers ensures that there are only two distinct H_2O monomer environments: one in which the monomer donates two hydrogen-bonds and accepts one (ADD), the other in which it accepts two and donates one (DAA).[50] The instanton tunneling paths and splitting patterns were computed for both isomers, as described below.

Instanton Tunneling Pathways. The TTM3-F[51] flexible water potential was used, which has been shown to give estimates of the correct order of magnitude for tunneling splittings in other water clusters.[40] This potential correctly identifies the two lowest minima with point groups D_{2d} and S_4; the D_{2d} isomer is only 0.005 kJ/mol lower in energy, while other isomers lie much higher.[6,7,10,11,52] The harmonic frequencies were calculated for both isomers and produce harmonic zero-point vibrational energies within 5% of the values obtained from benchmark calculations.[18]

There are many possible tunneling pathways in the water octamer, and we analyze the number of symmetry-related wells using the molecular symmetry group. This group is the subgroup of permutation-inversion operations corresponding to pathways that are deemed to be "feasible", which means that they correspond to tunneling matrix elements $h_{\lambda\mu}$ that give rise to observable tunneling splittings.[48,53] Because of the mass terms in eq 4, any pathway which involves significant displacements of oxygen atoms will correspond to large values of the action $S_{\lambda\mu}$. The same is true for pathways that break covalent bonds and thus pass over high barriers or for pathways which necessitate the rearrangement of many hydrogen-bonds as would an interconversion between the S_4 and D_{2d} isomers. Such high action pathways are deemed unfeasible and are excluded from the calculation. The pathways that can be considered feasible in water octamer are those that rotate individual monomers, exchanging the two hydrogen atoms. These paths connect pairs of the symmetrically related potential wells associated with each D_{2d} or S_4 isomer. As explained above, there are only two nonsymmetry-related monomer environments for each isomer and therefore, as either of these monomers can rotate, only four distinct pathways need be considered: two for D_{2d} and two for S_4.

The four relevant pathways were optimized using the modified limited-memory Broyden–Fletcher–Goldfarb–Shanno (L-BFGS) algorithm[54,55] in OPTIM[56] which minimized the objective function given by eq 4. The first derivatives of the potential energy surface $V(x)$ were evaluated analytically, and the second derivatives (needed only once per minimization to calculate Φ) were obtained numerically. The initial starting point for each of the instanton tunneling paths was taken to be a path in which half the beads were placed at a position x^λ, located in well λ, and the other half at a position x^μ in well μ. The optimizer rapidly pulled the central beads out of the wells and distributed them over the barrier. The computation was straightforward for this system because none of the paths were found to involve significant rearrangements of the oxygen atoms.[40] The number of replicas, N, and imaginary time-duration, $\beta\hbar$, were chosen to be large enough to converge the actions $S_{\lambda\mu}$ to within about 1%. This level of convergence was sufficient to determine the order of magnitude of the tunneling matrix elements $h_{\lambda\mu}$, and hence the splitting patterns.

The resulting instanton tunneling pathways are illustrated in Figure 1, and Table 1 gives the computed values of the quantities $S_{\lambda\mu}$, Φ and $h_{\lambda\mu}$. The values of the tunneling matrix elements obtained are too small to give rise to experimentally measurable splitting patterns (see next section), and thus we did not try to obtain more accurate convergence of $h_{\lambda\mu}$, which could have been achieved by converging with respect to N and β, as in ref 39, and also by using a better potential energy surface.[57]

Table 1. The Action, $S_{\lambda\mu}$, Fluctuation Factor, Φ, and Tunneling Matrix Element, $h_{\lambda\mu}$, Defined in Eq 3, Corresponding to the Four Tunneling Pathways Shown in Figure 1 and Calculated Using $N = 32$ and $\beta\hbar = 5000$ a.u.

pathway	$S_{\lambda\mu}$ (a.u.)	Φ (a.u.)	$-h_{\lambda\mu}$ (cm^{-1})
D_{2d}(ADD)	33.98	23	3.9×10^{-11}
D_{2d}(DAA)	29.67	118	1.4×10^{-9}
S_4(ADD)	33.93	25	3.7×10^{-11}
S_4(DAA)	28.99	123	9.8×10^{-10}

The reason that the values of $h_{\lambda\mu}$ are relatively small is clear: at least two hydrogen-bonds have to be broken along each of the four tunneling paths. This effect leads to high values of the actions, $S_{\lambda\mu}$, and hence to small tunneling splittings. The DAA transitions are slightly more labile, probably because they do not move the free hydrogen atoms so far into the center of the cluster. The pathways are similar to the bifurcation pathways in water trimer, except that the latter break only one hydrogen-bond,[58−60] and thus have actions about half of those of the octamer.

Tunneling Splittings. Although the tunneling splittings are too small to be measured in current experiments, it may be useful for future studies to describe the resulting tunneling splitting pattern, which is easily obtained by diagonalizing the tunneling matrix **W** of eq 2. It is also useful to analyze the structure of this matrix using the molecular symmetry group.[48,53] For this analysis, we will refer to a "structure" as a particular molecular geometry, and a "version" as a particular labeled permutational isomer.[61] Versions are said to be "adjacent" if they are directly connected by a single kink on the potential energy surface. The largest tunneling splittings

dx.doi.org/10.1021/jp311306a | J. Phys. Chem. A XXXX, XXX, XXX−XXX

usually correspond to "degenerate" rearrangements,[62] which connect distinct permutation-inversion isomers of the same structure.

The adjacency matrix **A**, and hence the splitting patterns, were calculated using the MS program,[63] which constructs the molecular symmetry group from a minimal set of generator operations. However, in this case, the adjacency matrix has quite a simple structure, and it was not a difficult task to check the result by labeling the 256 wells that are connected and identifying the adjacent wells directly. The tunneling matrix **W** is then constructed using the calculated matrix elements for kinks between adjacent versions.[40,61,64] For the S_4 isomer we consider the additional generator operations, $\mathcal{P}_{ADD}$ and $\mathcal{P}_{DAA}$, corresponding to exchange of protons in either an ADD or a DAA molecule. Because the instanton calculations indicate that there are two equivalent paths in each case, due to clockwise or anticlockwise rotation, we take the same value of h for each one, which is equivalent to using a single generator with matrix element $2h$.

Considering either $\mathcal{P}_{ADD}$ or $\mathcal{P}_{DAA}$, there are four symmetry equivalent operations corresponding to the four ADD or DAA molecules. The resulting molecular symmetry group contains 64 operations and has 13 classes: two of size 1, one of size 2, five of size 4, and five of size 8. These operations link versions in sets of 16, and each version is linked to four others by tunneling pathways, giving the splitting pattern

$$8h(1),\ 4h(4),\ 0(6),\ -4h(4),\ -8h(1)$$

where the degeneracies are in brackets. Here h is either h_{ADD} or h_{DAA}, as appropriate, and the energy level spacing is doubled by the two equivalent pathways corresponding to each monomer rotation. The largest eigenvalue simply reflects the connectivity of the reaction graph, and the symmetrical spacing about zero indicates that the graph contains no odd-membered rings.[65]

When both $\mathcal{P}_{ADD}$ and $\mathcal{P}_{DAA}$ are included, the molecular symmetry group expands to 1024 operations, which link versions in sets of 256. The group has 88 classes: four of size 1, six of size 2, sixty of size 4, four of size 16, six of size 32, and eight of size 64. Each version is connected to eight others, so the largest eigenvalue in the tunneling problem is $16h$ if each monomer has two proton exchange pathways, each contributing a matrix element h. In this case, the splitting pattern is

$$16h(1),\ 12h(8),\ 8h(28),\ 4h(56),\ 0(70),\ -4h(56),\ -8h(28),\ -12h(8),\ -16h(1)$$

In fact, the instanton calculations suggest that $h_{DAA} > h_{ADD}$. If we distinguish the two matrix elements then the splitting pattern, with degeneracies in brackets, becomes

$$8h_{DAA} + 8h_{ADD}(1),\ 8h_{DAA} + 4h_{ADD}(4),\ 8h_{DAA}(6),\ 8h_{DAA} - 4h_{ADD}(4),\ 8h_{DAA} - 8h_{ADD}(1),\ 4h_{DAA} + 8h_{ADD}(4),\ 4h_{DAA} + 4h_{ADD}(16),\ 4h_{DAA}(24),\ 4h_{DAA} - 4h_{ADD}(16),\ 4h_{DAA} - 8h_{ADD}(4),\ 8h_{ADD}(6),\ 4h_{ADD}(24),\ 0(36),$$

$$-4h_{ADD}(24),\ -8h_{ADD}(6),\ -4h_{DAA} + 8h_{ADD}(4),\ -4h_{DAA} + 4h_{ADD}(16),\ -4h_{DAA}(24),\ -4h_{DAA} - 4h_{ADD}(16),\ -4h_{DAA} - 8h_{ADD}(4),\ -8h_{DAA} + 8h_{ADD}(1),\ -8h_{DAA} + 4h_{ADD}(4),\ -8h_{DAA}(6),\ -8h_{DAA} - 4h_{ADD}(4),\ -8h_{DAA} - 8h_{ADD}(1)$$

This sequence corresponds to the case when h_{DAA} is assumed to be an order of magnitude or more greater than h_{ADD}. Setting $h_{DAA} = h_{ADD}$ recovers the pattern for identical matrix elements, and setting either h_{DAA} or h_{ADD} to zero recovers the single generator pattern. The symmetrical splitting about zero again indicates that the corresponding reaction graph contains no odd-membered rings.[65]

For the D_{2d} isomer, adding either the generator for $\mathcal{P}_{ADD}$ or $\mathcal{P}_{DAA}$ to the rigid molecule group produces a molecular symmetry group of order 128 with 20 classes: two of size 1, one of size 2, nine of size 4, five of size 8, and three of size 16. Versions are linked in sets of 16 by these operations, and the reaction graph has a connectivity of four. The resulting splitting pattern is the same as for the S_4 isomer.

When both $\mathcal{P}_{ADD}$ and $\mathcal{P}_{DAA}$ are included, the molecular symmetry group expands to order 2048, with 119 classes: four of size 1, six of size 2, 30 of size 4, 31 of size 8, 28 of size 16, 10 of size 32, six of size 64, and four of size 128. These operations link versions in sets of 256 giving a reaction graph with connectivity 8. The splitting pattern is again the same as for the S_4 isomer. Further details of the molecular symmetry groups are omitted for brevity, but are available from the authors. Using the values of the matrix elements h_{DAA} and h_{ADD} given in Table 1 for either isomer in eq 5 yields a tunneling splitting pattern for which the difference between the highest and lowest energy levels is of order 2×10^{-8} cm^{-1}. This is too small to be resolved by existing experimental techniques, and because interconversion between the isomers is also unfeasible, we expect both the D_{2d} and the S_4 isomers to exhibit spectra corresponding to semirigid symmetric top molecules.

Experimental Measurements on the Water Octamer. The Berkeley Terahertz Spectrometer[66−68] was used in conjunction with a variable field Putley-mode (VFP) detector[69−72] in an effort to locate VRT transitions of the water octamer in the previously unscanned region between 1.35 and 1.8 THz. Jet-cooled H_2O clusters were formed in the usual way by bubbling argon at a backing pressure of 17−18 psi through a reservoir of distilled room-temperature H_2O, and subsequently expanding the saturated carrier gas through the pulsed planar supersonic expansion source discussed in refs 69−72. Argon was used as the primary carrier gas in these experiments in order to maximize the chance of observing tunneling fine structure, since it produces narrower residual Doppler linewidths than He or Ne. The data collection scheme was used as described in refs 69−72. and each data point collected represents an average over 32 gas pulses.

Figure 2 displays what is tentatively assigned as a spectrum belonging to the h16-water octamer, comprising 77 weak lines centered at about 1383.32 GHz (46.11 cm^{-1}) and measured with an average signal-to-noise ratio of 8:1, with the most intense transition reaching 30:1. Transition frequencies and relative intensities are presented in the Supporting Information. A single far-infrared laser with a center frequency of 1397.1186 GHz (46.6029 cm^{-1} CH_2F_2) was sufficient for observing all of these transitions. Similar to the transitions observed for other water clusters generated in Ar expansions,[1,69−72] the lines measured in this band had a full-width at half-maximum of 700 kHz. However, unlike other such bands, the transitions were spaced very close together (often within 2 to 3 MHz). The microwave frequency modulation depth was varied in order to resolve any possible tunneling splittings in the individual lines of this band. However, all observed transitions appeared as singlets with no discernible fine structure.

dx.doi.org/10.1021/jp311306a | J. Phys. Chem. A XXXX, XXX, XXX−XXX

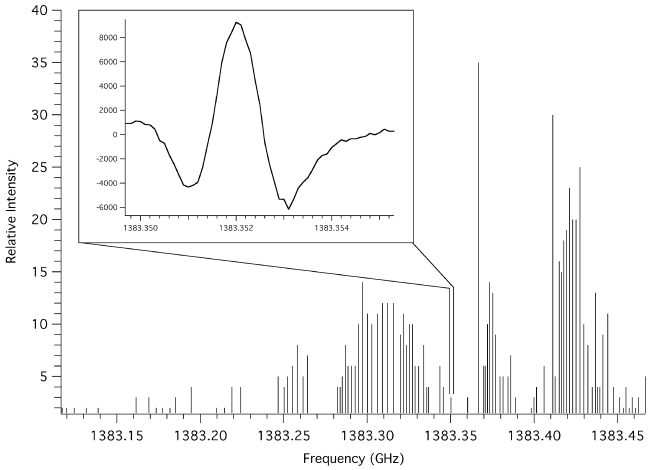

Figure 2. Stick spectrum of the 77 transitions, measured to sub-MHz precision. All transitions appear as singlets, without resolvable structure, as shown for one transition in the inset. Frequencies are given in GHz.

In order to provide some evidence for the identity of the spectral carrier, isotope dilution experiments were performed.[1,69−72] Three strong transitions were chosen from the cluster of lines for this experiment, and each of these peaks was tested five times with five different H_2O/D_2O mixtures; 98%, 97%, 96%, 94%, and 92% H_2O, as well as with a pure H_2O sample, using distilled H_2O in conjunction with D_2O (Cambridge Isotopes, 99.9% pure). The relative intensities for each isotopic mix were averaged, and the results were plotted in Figure 3. The number of water molecules in the

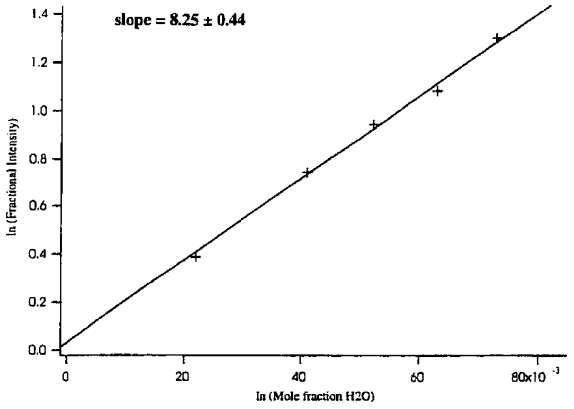

Figure 3. The results of the isotopic substitution experiment for the partial band centered at 1383.32 GHz (46.11 cm^{-1}). Each of the five data points represents the average for three different measured transitions. The slope of this graph indicates that the spectral carrier is the water octamer.

spectral carrier was calculated to be eight at 95% confidence. Therefore, the results of the isotope experiment indicate that these transitions belong to a rovibrational transition of the h16-water octamer.

In an effort to extend this band, a range of over 2 cm^{-1} (60 GHz) was scanned on either side of the originally measured transitions. While numerous lines belonging to argon−water clusters were measured in these data, none of the peaks yielded the same isotope experiment results as the transitions discussed above. Therefore, while it appears likely that the observed spectra comprise the first VRT transitions observed for the water octamer, any additional lines for this band almost certainly lie below the current experimental detection limit of the spectrometer.

As described above, calculations predict a symmetric top spectrum for both the D_{2d} and S_4 structures; the O−O distances between the two tetramer rings that comprise the octamer are calculated as 2.83 Å,[24,25] longer than two of the four connections (2.64 Å) within the individual tetramers. Interestingly, the same DFT calculations predict a prolate symmetric top for the S_4 structure, but an oblate top for the D_{2d} geometry, as a result of switching the location of the long and short hydrogen-bonds in each of the two tetramer subunits.

Initially, it was not clear whether some of the observed very dense spectral structure was a result of complicated tunneling splittings, but the calculations presented earlier in this paper strongly suggest that such splittings are too small to be observed in the present experiment. Hence, our focus in assigning the spectra shifted to the rotational structure of a symmetric rotor. Assuming the inertial structure of the water octamer to be a semirigid symmetric top, then the measured spectrum presented in Figure 2 is likely to be the most intense region of the Q-branch. As a test of this model, the rotational constants calculated by Gruenloh et al.[24,25] were used to simulate a vibration−rotation band for the D_{2d} structure, the lowest energy isomer of the two cubic water octamer structures. The simulated transitions were calculated using a Watson S-reduced Hamiltonian, including up to sextic distortion constants and Boltzmann weighted intensities with a temperature of 5 K, typical for water clusters formed in Ar molecular beams; transitions were calculated for J and K values from 0 to 15. The excited state rotational constants, as well as the distortion constants, for these simulations were estimated using the same ΔA, ΔB, and so on values determined by Liu et al.[73] for the water hexamer. The results of this simulation for the D_{2d} structure are shown in Figure 4. Since the calculated b- and c-type spectra are identical, the latter are not shown in this figure.

Because the observed lines span a region of only 350 MHz, it is assumed that if this rovibrational band did indeed arise from a symmetric rotor structure for the water octamer, then the measured transitions most likely belong to the Q-branch, since the Q-branch for symmetric rotors is typically very compact. Furthermore, Q-branch transitions are usually more intense than P- or R-branch lines, and since no other transitions corresponding to water octamer lines were observed, these features are most likely the strongest transitions in this band. A magnified plot of the simulated symmetric rotor Q-branch region for both a-type and b-type transitions is shown at the top of Figure 4 for comparison with the experimentally measured lines. As illustrated in this figure, the a-type Q-branch spectrum does not actually match the line density of the observed transitions nearly as well as the simulated b-type spectrum. Hence, while the actual line spacing of the simulated b-type Q-branch does not match well to the experimental lines, it is most likely that this new band belongs to a b-type (or c-type) transition. These simulations were also useful in predicting the possible locations of the P- and R-branch progressions in the data set. Accordingly, the entire simulated band for the b-type transition of the water octamer is plotted at the bottom of Figure 4.

DISCUSSION

A new rovibrational band, centered at 1383.32 GHz (46.11 cm^{-1}), has been measured with the Berkeley Terahertz VRT

dx.doi.org/10.1021/jp311306a | J. Phys. Chem. A XXXX, XXX, XXX−XXX

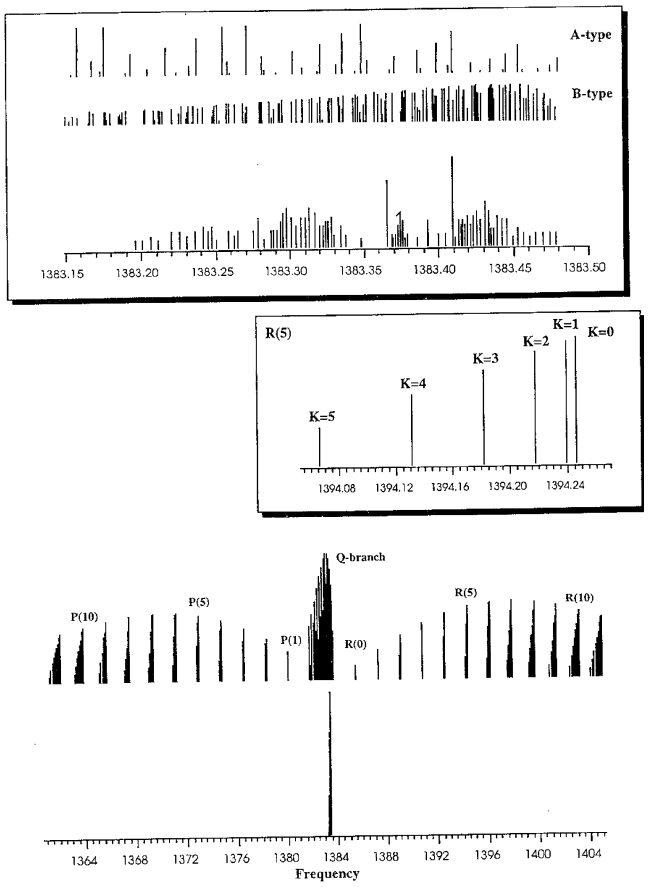

Figure 4. Simulated vibration−rotation band for the D_{2d} structure of the water octamer. Excited state constants were calculated using the same ΔA, ΔB, and ΔC values as measured for the water hexamer. A temperature of 5 K is assumed. The bottom graph shows the entire simulated b-type spectrum for the D_{2d} structure of the water octamer compared to the experimentally measured lines. The middle plot illustrates the R(5) branch for this same simulation and shows the typical K-stack progression for a symmetric top. The top graph in this figure compares the Q-branch regions for the calculated a-type and b-type transitions (the c-type simulations are identical to the b-type) with the experimentally measured lines for this cluster, shown at the bottom of this graph. Frequencies are given in GHz.

Spectrometer. While isotope dilution experiments on several lines of this band have provided reasonably convincing evidence that it belongs to the h16-water octamer, much of the spectrum most likely still lies below the experimental detection limit. Symmetric top simulations performed for the lowest energy (D_{2d}) structure suggest that this band could belong to a b- or c-type transition. The overall agreement in line spacings between the simulated spectra and the experimentally observed transitions was not good, but this model employed excited state parameters from water hexamer spectra, which may not be representative of this octamer transition.

It is probable that the observed lines are part of the strong Q-branch transitions of a symmetric rotor, and that the P- and R-branch lines, which may be separated from the band origin by several gigahertz if Coriolis effects are present, have not yet been measured due to their comparatively low signal-to-noise ratio. However, since the D_{2d} and S_4 structures of the water octamer lie so close in energy, it is possible that both are observed in the molecular beam and that both have vibrations in this area. This possibility would further complicate the assignment of the transitions measured in this region, and a detailed analysis would certainly require a more complete picture of the remaining lines of this band.

CONCLUSIONS

A set of transitions observed near 1.4 THz in a supersonic expansion of H_2O in argon are tentatively assigned to a Q-branch of the water octamer-h16 on the basis of isotope dilution experiments and a detailed analysis of expected tunneling splittings, which lie below the current experimental resolution. This result implies a simple relationship between the number of hydrogen-bonds broken and the magnitude of the tunneling splitting, so that it should be easy to predict which water clusters will give an observable splitting pattern and which will not. For example, we expect that the water heptamer and nonamer should show tunneling splittings, but it is unlikely that the dodecamer will.

ASSOCIATED CONTENT

Supporting Information

Observed frequencies and intensities of the VRT band. This material is available free of charge via the Internet at http://pubs.acs.org.

AUTHOR INFORMATION

Corresponding Author

*E-mail: sca10@cam.ac.uk (S.C.A.); saykally@berkeley.edu (R.J.S.).

Present Addresses

[§]Friedrich-Alexander-Universität Erlangen-Nürnberg, Staudtstraß e 7/B2, D-91058 Erlangen, Germany.

[∥]Department of Chemistry, Seattle University, Seattle, WA 98122-1090

[⊥]School of Biosciences, University of Birmingham, Edgbaston, Birmingham, B15 2TT, United Kingdom.

Notes

The authors declare no competing financial interest.

ACKNOWLEDGMENTS

J.O.R. was supported by a doctoral training award from the U.K. Engineering and Physical Sciences Research Council. The Berkeley Terahertz experiments were supported by the National Science Foundation (Grant #CHE1011825).

REFERENCES

(1) Keutsch, F. N.; Saykally, R. J. *Proc. Natl. Acad. Sci. U.S.A.* **2001**, *98*, 10533−10540.
(2) Cohen, R. C.; Saykally, R. J. *J. Phys. Chem.* **1992**, *96*, 1024−1040.
(3) Pugliano, N.; Saykally, R. J. *J. Chem. Phys.* **1992**, *96*, 1832−1839.
(4) Saykally, R. J.; Blake, G. A. *Science* **1993**, *259*, 1570−1575.
(5) Liu, K.; Cruzan, J. D.; Saykally, R. J. *Science* **1996**, *271*, 929−932.
(6) Tsai, C. J.; Jordan, K. D. *J. Chem. Phys.* **1991**, *95*, 3850−3853.
(7) Tsai, C. J.; Jordan, K. D. *J. Chem. Phys.* **1993**, *99*, 6957−6970.
(8) Stillinger, F. H.; David, C. W. *J. Chem. Phys.* **1980**, *73*, 3384−3389.
(9) Brink, G.; Glasser, L. *J. Phys. Chem.* **1984**, *88*, 3412−3414.
(10) Wales, D. J.; Ohmine, I. *J. Chem. Phys.* **1993**, *98*, 7245−7256.
(11) Wales, D. J.; Ohmine, I. *J. Chem. Phys.* **1993**, *98*, 7257−7268.
(12) Nigra, P.; Carigano, M. A.; Kais, S. *J. Chem. Phys.* **2001**, *115*, 2621−2628.
(13) Tharrington, A. N.; Jordan, K. D. *J. Phys. Chem. A* **2003**, *107*, 7380−7389.
(14) Kim, J.; Kim, B. J.; Lee, S. J.; Kim, K. *Chem. Phys. Lett.* **1994**, *219*, 243−246.

(15) Kryachko, E. S. *Int. J. Quantum Chem.* **1998**, *70*, 831−853.
(16) Dang, L. X. *J. Chem. Phys.* **1999**, *110*, 1526−1532.
(17) Kim, J.; Majumdar, D.; Lee, H. M.; Kim, K. S. *J. Chem. Phys.* **1999**, *110*, 9128−9134.
(18) Xantheas, S. S.; Apra, E. *J. Chem. Phys.* **2004**, *120*, 823−828.
(19) Jorgensen, W. L.; Chandrasekhar, J.; Madura, J. D.; Impey, R. W.; Klein, M. L. *J. Chem. Phys.* **1983**, *79*, 926−935.
(20) Hernández-Rojas, J.; Gonzalez, B. S.; James, T.; Wales, D. J. *J. Chem. Phys.* **2006**, *125*, 224302.
(21) Ocasio, M.; Lopez, G. E. *Chem. Phys. Lett.* **2002**, *356*, 168−174.
(22) Miyake, T.; Aida, M. *Chem. Phys. Lett.* **2006**, *427*, 215−220.
(23) Asare, E.; Musah, A. R.; Curotto, E.; Freeman, D. L.; Doll, J. D. *J. Chem. Phys.* **2009**, *131*, 184508.
(24) Gruenloh, C. J.; Carney, J. R.; Arrington, C. A.; Zwier, T. S.; Fredericks, S. Y.; Jordan, K. D. *Science* **1997**, *276*, 1678−1681.
(25) Gruenloh, C. J.; Carney, J. R.; Hagemeister, F. C.; Arrington, C. A.; Zwier, T. S.; Fredericks, S. Y.; Wood, J. T.; Jordan, K. D. *J. Chem. Phys.* **1998**, *109*, 6601−6614.
(26) Suitte, B. P.; Belair, S. D.; Francisco, J. S. *Phys. Rev. A* **2005**, *71*, 043204.
(27) Blanton, W. B.; Gordonwylie, S. W.; Clark, G. R.; Jordan, K. D.; Wood, J. T.; Geiser, U.; Collins, T. J. *J. Am. Chem. Soc.* **1999**, *121*, 3551−3552.
(28) Prasad, T. K.; Rajasekharan, M. V. *Cryst. Growth Des.* **2006**, *6*, 488−491.
(29) Hao, H.-J.; Sun, D.; Liu, F.-J.; Huang, R.-B.; Zheng, L.-S. *Cryst. Growth Des.* **2011**, *11*, 5475−5482.
(30) Sun, Y.-G.; Gao, E.-J.; Wei, D.-Z. *Inorg. Chem. Commun.* **2007**, *10*, 467−470.
(31) Katada, H.; Seino, H.; Mizobe, Y.; Sumaoka, J.; Komiyama, M. *J. Biol. Inorg. Chem.* **2008**, *13*, 249−255.
(32) Svoboda, O.; Oncak, M.; Slavicek, P. *J. Chem. Phys.* **2011**, *135*, 154301.
(33) Lee, H. M.; Kim, K. S. *J. Chem. Phys.* **2002**, *117*, 706−708.
(34) Vaitheeswaran, S.; Yin, H.; Rasaiah, J. C.; Hummer, G. *Proc. Natl. Acad. Sci. U.S.A.* **2004**, *101*, 17002−17005.
(35) James, T.; Wales, D. J.; Hernández-Rojas, J. *J. Chem. Phys.* **2007**, *126*, 054506.
(36) Ludwig, R. *Angew. Chem., Int. Ed.* **2001**, *40*, 1808−1827.
(37) Svozil, D.; Jungwirth, P. *J. Phys. Chem. A* **2006**, *110*, 9194−9199.
(38) Fredericks, S. Y.; Jordan, K. D. *Mol. Phys.* **1997**, *92*, 445−448.
(39) Richardson, J. O.; Althorpe, S. C. *J. Chem. Phys.* **2011**, *134*, 054109.
(40) Richardson, J. O.; Althorpe, S. C.; Wales, D. J. *J. Chem. Phys.* **2011**, *135*, 124109.
(41) Vainshtein, A. I.; Zakharov, V. I.; Novikov, V. A.; Shifman, M. A. *Sov. Phys. Usp.* **1982**, *25*, 195. Also in *Instantons in Gauge Theories*; Shifman, M., Ed.; World Scientific: Singapore, 1994; p 468.
(42) Benderskii, V. A.; Makarov, D. E.; Wight, C. A. *Chemical Dynamics at Low Temperatures*; Wiley: New York, 1994; Vol. *88*.
(43) Mil'nikov, G. V.; Nakamura, H. *J. Chem. Phys.* **2001**, *115*, 6881−6897.
(44) Rommel, J. B.; Kästner, J. *J. Chem. Phys.* **2011**, *134*, 184107.
(45) Smedarchina, Z.; Siebrand, W.; Zgierski, M. Z.; Zerbetto, F. *J. Chem. Phys.* **1995**, *102*, 7024−7034.
(46) Makri, N.; Miller, W. H. *J. Chem. Phys.* **1989**, *91*, 4026−4036.
(47) Miller, W. H. *J. Chem. Phys.* **1975**, *62*, 1899−1906.
(48) Longuet-Higgins, H. C. *Mol. Phys.* **1963**, *6*, 445−460.
(49) Shank, A.; Wang, Y.; Kaledin, A.; Braams, B. J.; Bowman, J. M. *J. Chem. Phys.* **2009**, *130*, 144314.
(50) Buck, U.; Ettischer, I.; Melzer, M.; Buch, V.; Sadlej, J. *Phys. Rev. Lett.* **1998**, *80*, 2578−2581.
(51) Fanourgakis, G. S.; Xantheas, S. S. *J. Chem. Phys.* **2008**, *128*, 074506.
(52) Maeda, S.; Ohno, K. *J. Phys. Chem. A* **2007**, *111*, 4527−4534.
(53) Bunker, P. R.; Jensen, P. *Molecular Symmetry and Spectroscopy*, 2nd ed.; NRC Research Press: Ottawa, ON, Canada, 1998.
(54) Nocedal, J. *Math. Comput.* **1980**, *35*, 773−782.
(55) Liu, D. C.; Nocedal, J. *Math. Program* **1989**, *45*, 503−528.
(56) Wales, D. J. *OPTIM, A Program for Optimizing Geometries and Calculating Pathways*. http://www-wales.ch.cam.ac.uk/software.html
(57) Wang, Y.; Shepler, B. C.; Braams, B. J.; Bowman, J. M. *J. Chem. Phys.* **2009**, *131*, 054511.
(58) Wales, D. J. *J. Am. Chem. Soc.* **1993**, *115*, 11180−11190.
(59) Walsh, T. R.; Wales, D. J. *J. Chem. Soc., Faraday Trans.* **1996**, *92*, 2505−2517.
(60) Keutsch, F. N.; Saykally, R. J.; Wales, D. J. *J. Chem. Phys.* **2002**, *117*, 8823−8835.
(61) Bone, R. G. A.; Rowlands, T. W.; Handy, N. C.; Stone, A. J. *Mol. Phys.* **1991**, *72*, 33−73.
(62) Leone, R. E.; von R. Schleyer, P. *Angew. Chem., Int. Ed.* **1970**, *9*, 860−890.
(63) Wales, D. J. *MS: a program for finding molecular symmetry groups and tunnelling splitting patterns.*
(64) Wales, D. J. *J. Am. Chem. Soc.* **1993**, *115*, 11191−11201.
(65) Coulson, C. A.; Rushbrooke, S. *Proc. Cambridge Philos. Soc.* **1940**, *36*, 193−200.
(66) Blake, G. A.; Laughlin, K. B.; Cohen, R. C.; Busarow, K. L.; Gwo, D. H.; Schmuttenmaer, C. A.; Steyert, D. W.; Saykally, R. J. *Rev. Sci. Instrum.* **1991**, *62*, 1701−1716.
(67) Liu, K.; Fellers, R. S.; Viant, M. R.; McLaughlin, R. P.; Brown, M. G.; Saykally, R. J. *Rev. Sci. Instrum.* **1996**, *67*, 410−416.
(68) Brown, M. G.; Keutsch, F. N.; Braly, L. B.; Saykally, R. J. *J. Chem. Phys.* **1999**, *111*, 7801−7806.
(69) Cruzan, J. D.; Brown, M. G.; Liu, K.; Braly, L.; Saykally, R. *J. Chem. Phys.* **1996**, *105*, 6634−6644.
(70) Harker, H. A.; Viant, M. R.; Keutsch, F. N.; Michael, E. A.; McLaughlin, R. P.; Saykally, R. J. *J. Phys. Chem. A.* **2005**, *109*, 6483−6497.
(71) McLaughlin, R. P. Ph.D. Thesis, University of California-Berkeley, 1999.
(72) Lin, W.; Han, J.-X.; Takahashi, L. K.; Harker, H. A.; Keutsch, F. N.; Saykally, R. J. *J. Chem. Phys.* **2008**, *128*, 094302.
(73) Liu, K.; Brown, M. G.; Saykally, R. J. *J. Phys. Chem. A* **1997**, *101*, 8995−9010.